



Phosphate depletion controls lipid content and accumulation of heterotrophic bacteria during growth of *Synechocystis* sp. PCC 6803

Yun Zhou^{1,2,3} · YenJung Sean Lai¹ · Everett Eustance¹ · Siqing Xia² · Bruce E. Rittmann¹

Received: 23 February 2019 / Revised: 26 March 2019 / Accepted: 31 March 2019 / Published online: 27 April 2019
© Springer-Verlag GmbH Germany, part of Springer Nature 2019

Abstract

During the culturing of cyanobacteria, heterotrophic bacteria can compete for nutrients, compromise the quality of the harvested biomass, or cause culture crashes. We systematically investigated the effects of depleting inorganic phosphate (Pi) on the growth of the cyanobacterium *Synechocystis* sp. PCC 6803, its community of heterotrophic bacteria, and the biomass's chemical composition. On the one hand, depleting Pi had minimal impact on total biomass, extracellular polymeric substances (ESP), soluble microbial products (SMP), and most types of intracellular organic polymers production. On the other hand, depleting Pi led to markedly less lipid content, less heterotrophic biomass, and a shift in the heterotrophic community from *Burkholderiales* to *Spingobacteriales* and *Saprospirales*. The causes of the large impacts were that *Synechocystis* was much better at scavenging a very low Pi concentration and lowering the Pi available to the heterotrophs. This work lays a foundation for controlling the accumulation of heterotrophs and reducing their deleterious effects in cyanobacteria culturing.

Keywords Phosphate · Batch experiment · Heterotrophic bacteria · *Synechocystis* sp. PCC 6803 · Microbial community

Introduction

In a cyanobacteria-based photobioreactor (PBR), cyanobacteria-generated soluble microbial products (SMPs) and extracellular polymeric substances (EPSs) can become sources of carbon and electrons for heterotrophic bacteria (Nguyen and Rittmann 2016b; Zevin et al. 2015). SMPs are

direct electron-donor substrates for heterotrophic bacteria (Laspidou and Rittmann 2002). As one of the important SMP sources, EPS are indirect substrates for heterotrophic bacteria. Decho et al. (2005) found that cyanobacterial EPS was rapidly transformed post-secretion through heterotrophic degradation, resulting in growth of heterotrophs, along with the accumulation of refractory remnant polymers.

Heterotrophic bacteria in a PBR may influence the growth of cyanobacteria, more often in negative ways. Some heterotrophic bacteria can cause the lysis of cyanobacterial cells through enzymatic or antibiotic action, which is directly detrimental to biomass productivity (Rashidan and Bird 2001; Zhang et al. 2018; Zhou et al. 2017a), others can consume valuable organic products excreted by cyanobacteria (Zevin et al. 2015), and competition for nutrients may lower the growth rate and yield of cyanobacteria (Straka and Rittmann 2017). Studying how heterotrophic bacteria affected inorganic phosphorus (Pi) stress to *Synechocystis* sp. PCC 6803, Straka and Rittmann (2017) found that heterotrophic bacteria contained about half of the culture's inorganic phosphorus (Pi), even though *Synechocystis* dominated the total biomass. The sequestration of P by the heterotrophs led to a roughly 50% decrease in *Synechocystis* production.

Electronic supplementary material The online version of this article (<https://doi.org/10.1007/s00253-019-09817-9>) contains supplementary material, which is available to authorized users.

✉ Siqing Xia
siqingxia@tongji.edu.cn

✉ Bruce E. Rittmann
rittmann@asu.edu

¹ Biodesign Swette Center for Environmental Biotechnology, Arizona State University, Tempe, AZ 85287-5701, USA

² State Key Laboratory of Pollution Control and Resource Reuse, College of Environmental Science and Engineering, Tongji University, Shanghai 200092, China

³ Department of Civil and Environmental Engineering, University of Alberta, 7-263 Donadeo Innovation Center for Engineering, Edmonton, Alberta T6G 1H9, Canada

Phosphorus is a key component of phospholipids, and the availability of Pi affects the accumulation of lipids (Juneja et al. 2013). For example, Pi starvation shifts lipid metabolism from membrane lipid synthesis to neutral lipid storage and, in turn, increases the total lipid content of green algae (Hu 2004; Xin et al. 2010). Although cyanobacteria do not accumulate neutral lipids, the loss of membrane lipids seems to be an outcome of Pi depletion.

In this study, we used centrifugation- and thermal-based methods to separate SMP, EPS, and intracellular polymeric substances (IPSs) from biomass grown in batch cultures in which *Synechocystis* sp. PCC 6803 was the photosynthetic primary producer. Combining those measurements with microbial community analyses allowed us to observe how Pi influenced the accumulation of lipids and differentially affected heterotrophs versus *Synechocystis* during batch growth.

Methods and materials

***Synechocystis* cultures and batch growth experiments** Wild-type *Synechocystis* sp. PCC 6803 (hereafter *Synechocystis*) was maintained in 500-mL Erlenmeyer flasks with a working volume of 300 mL and incident light intensity of $\sim 80 \mu\text{mol photons m}^{-2} \text{s}^{-1}$, utilizing standard BG-11 (Rippka et al. 1979), and bubbled with air filtered through a 1.0- μm air filter (Pall, Port Washington, NY, USA). An aliquot from a flask culture with the optical density (OD) of 3.4 after incubated for 7-day was diluted to an OD of 0.6 ± 0.02 to initiate each batch growth experiment.

The setup of the PBR used in the batch growth experiment is shown in Fig. S1, and the culturing conditions in the batch experiments were as follows: working volumes of 700 mL using 1-L Erlenmeyer flasks; temperature of $30 \pm 0.8 \text{ }^\circ\text{C}$, maintained by $3 \times 12\text{-W}$ automated-air fans (Minebea-Matsushita Motor Corp., Japan) (Nguyen and Rittmann 2016a); incident light intensity of $276 \mu\text{mol photons m}^{-2} \text{s}^{-1}$, maintained by T5 fluorescent plant-grow lamps (Envirogro Hydrofarm, USA); pH of 8.0, maintained by a pH-Stat that initiated pure CO_2 sparging when the pH rose above 8.01 (Nguyen and Rittmann 2015); and culture mixing by sparging continuously with humidified air (bubbled through deionized water and filtered through a 1.0- μm air filter (Pall, Port Washington, NY, USA)). The starting alkalinity was augmented by adding 6.0 mM of bicarbonate (as NaHCO_3). Baseline NO_3^- and PO_4^{3-} concentrations were 8.6 mM (120 mg N/L) and 0.39 mM (12 mg P/L), consistent with the stoichiometric ratio of 22 mol N/mol P in standard BG-11 medium (Zhou et al. 2017c). The low-P condition had a starting P concentration to 0.055 mM (1.69 mgP/L, 3.1 mol N/mol P). All constituents other than N, P, and alkalinity were the same as standard BG-11. Prior to inoculation, the flasks and the BG-11 medium were

sterilized by autoclaving, and the pH probe was sterilized using 75% ethanol.

Extraction of extracellular and intracellular organic matter from *Synechocystis* As summarized in Fig. S2, centrifugation- and thermal-based methods were used to separate SMP, EPS, and IPSs from the mixed culture (Zhou et al. 2016; Zhou et al. 2017c). A biomass sample was centrifuged (Microfuge® 22R Centrifuge, Beckman Coulter, CA, USA) at $3600 \times g$ and $4 \text{ }^\circ\text{C}$ for 15 min, and the supernatant was further centrifuged (same centrifuge) at $10800 \times g$ and $4 \text{ }^\circ\text{C}$ for 10 min to further remove the particles. The final supernatant contained SMP. The pellets from both centrifugations were combined and resuspended to their original volumes using a pH-8.4 borate buffer (Wang et al. 2017). These suspensions were heated to $60 \text{ }^\circ\text{C}$, held there for 20 min, and then centrifuged at $3600 \times g$ at $4 \text{ }^\circ\text{C}$ for 15 min (Zhou et al. 2016). The supernatant was further centrifuged at $10,800 \times g$ at $4 \text{ }^\circ\text{C}$ for 10 min to remove particles, and this final supernatant contained the EPS. The pellets from the EPS step were resuspended to their original volumes using the borate buffer, and this suspension contained the IPS.

Fractionation of SMP and EPS into proteins and carbohydrates was carried out directly on these soluble materials. Fractionation of IPS required additional steps. For intracellular protein and carbohydrate, we mixed 1 mL of 0.5 M H_2SO_4 with 9 mL of IPS sample in 15-mL polypropylene centrifuge tubes (BD Falcon, VWR, USA). The mixture was subsequently shaken by hand and reacted for 4 h to dissolve the cell membrane, and the whole mixture was used for the assay of intracellular protein and carbohydrate. For intracellular chlorophyll and carotenoids, we mixed a 1-mL slurry containing $569 \pm 8.2 \text{ mg/L}$ of freeze-dried biomass containing only IPS (FreeZone Benchtop instrument (Labconco, MO, USA)) with 3 mL of Folch solvent (Chloroform/methanol = 2:1 v/v) in a 7.5-mL Pyrex disposable screw-cap culture tube (Gilbert-López et al. 2015). The mixture was subsequently shaken at 3200 rpm and $23 \text{ }^\circ\text{C}$ for 5 h on the Vortex-Genie 2 and then centrifuged at $3600 \times g$ and $23 \text{ }^\circ\text{C}$ for 10 min, and the supernatant was used for the assay of intracellular chlorophyll and carotenoid. For intracellular lipids, direct transesterification (DT) was carried out with a 1-mL slurry sample of freeze-dried biomass (FreeZone Benchtop instrument (Labconco, MO, USA)). Samples were amended with 2 mL of 3 N methanolic HCl (Sigma-Aldrich, MO, USA) and incubated at $85 \text{ }^\circ\text{C}$ in the oven for 2.5 h. The mixture was centrifuged at $3600 \times g$ and $23 \text{ }^\circ\text{C}$ for 10 min, and the supernatant was used for the assay of intracellular lipid.

Analytical methods Sample OD_{730} was measured with a UV-vis BioSpec-mini spectrometer at 730 nm (Shimadzu Corp., Japan). Dry weight (DW) was quantified using the total suspended solids assay, Method 2540D in *Standard Methods*

(Association 1998). We measured the protein present in SMP, EPS, and IPS with a QuantiPro BCA Assay Kit (Sigma-Aldrich, St. Louis, MO, USA) using bovine serum albumin (BSA) as the standard (Frølund et al. 1996). The carbohydrate content in SMP, EPS, and IPS was assayed with the phenol-sulfuric acid method using glucose as the standard (Dubois et al. 1956). The concentrations of chlorophyll and carotenoid were measured with a spectrophotometer (Bio Cary 50 – Varian, USA) based on the characteristic absorbances of the pigments (Gilbert-López et al. 2015): 470 and 665 nm for chlorophyll and carotenoid, respectively, and the standard curves are shown in our previous work (Zhou et al. 2017b). FAME components after direct transesterification were quantified using a gas chromatograph (Shimadzu GC 2010, Japan) equipped with a Supelco SP-2380 capillary column (30 m × 0.25 mm × 0.20 μm) and flame ionization detector (FID) (Sheng et al. 2011) against a 37-Component FAME Mix standard (Supelco, PA, USA).

Microbial community analyses: DNA extraction Pellets were prepared from the reactors at the end of batch operation. Approximately 0.30 g dry weight was used for DNA extraction with a PowerSoil DNA isolation kit (MoBio laboratories, Inc., Carlsbad, CA). We assessed the quantity and quality of extracted DNA by using a NanoDrop spectrophotometer (ND1000, ThermoFisher, MA) at 260 and 280 nm (Ruiz et al. 2014). The DNA concentrations and A260/A280 for all samples were higher than 178.2 ng/μL and 1.87, respectively.

Sequencing and bioinformatics analyses The DNA was sent to the Microbiome Analysis Laboratory (<http://krajmalnik.environmentalbiotechnology.org/microbiome-lab.html>) at Arizona State University (AZ, USA) for bar-coded amplicon sequencing. Triplicate PCR amplifications were performed for each sample and targeted the V4 region of the 16S rRNA gene with primer set 515f/806r (Caporaso et al. 2012). DNA samples were analyzed by a MiSeq Illumina sequencer and Illumina chemistry version 2 (2 × 150 paired-end). Analysis of the 16S rRNA gene sequences was performed using the Quantitative Insights into Microbial Ecology software package (QIIME, version 1.9) (Caporaso et al. 2010). 16S rRNA gene sequences were clustered into OTUs (operational taxonomy units) according to the Greengenes database using an identity threshold of 97% by using the UCLUST algorithm (Edgar 2010). Representative sequences for each OTU were aligned with the Greengenes core reference alignment (Caporaso et al. 2009) using PYNAST (DeSantis et al. 2006). The taxonomy of the OTU representative sequences was classified by RDP CLASSIFIER v.2.2 (Wang et al. 2007). After alignment of the sequences, we constructed an OTU table and removed singletons. Finally, the OTU table was rarefied to the minimum number of sequences (34351)

obtained among the samples. Sample sequences were deposited at the NCBI/Sequence Read Archive (SRA) under project SRP136645 with accession numbers of SAMN08802819–SAMN08802827, which were represented for the samples of control, H2, H4, H6, H8, L2, L4, L6, and L8, respectively. Control means the starting inoculum; H2–H8 and L2–L8 represent the samples after incubated for 2–8 days with the starting P concentration to 0.39 and 0.055 mM, respectively.

Statistical analyses For the batch growth experiments, we took triplicate samples from the reactor at the noted times, and each sample was assayed one time for OD₇₃₀, DW, NO₃⁻, PO₄³⁻, SMP, EPS, IPS, protein, carbohydrate, chlorophyll, carotenoid, and lipids as FAME. Results are expressed as the mean and standard deviation of the three measured samples (mean ± SD).

Results

Biomass growth and nutrient utilization Figure 1 shows the concentrations of biomass, NO₃⁻-N, and PO₄³⁻-P in the bulk solution for the batch experiments having two initial Pi

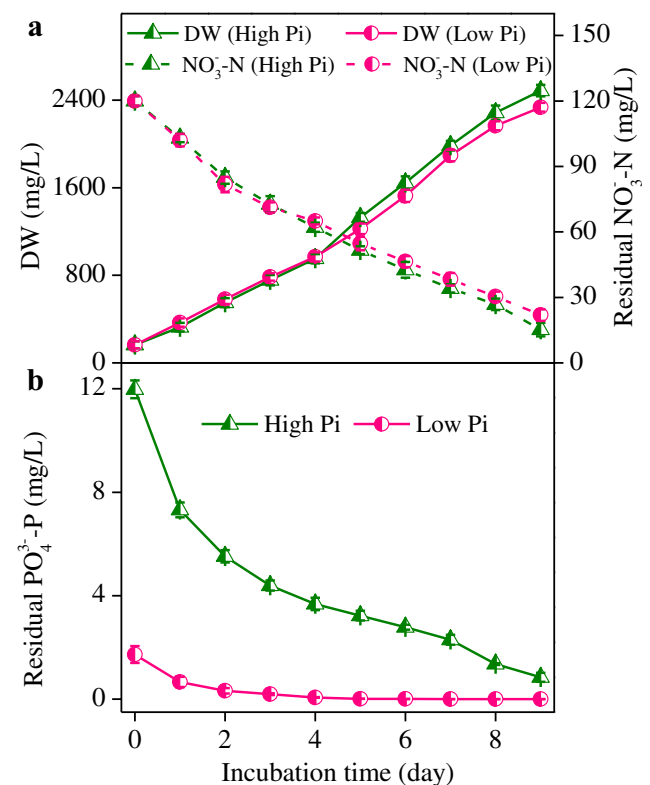


Fig. 1 Biomass production and nutrient utilization for batch experiments with high or low inorganic phosphate (Pi). DW dry weight of biomass. The symbols and bars show is the mean ± SD for $n = 3$; non-visible bars indicate that the SD is smaller than the size of the symbol

concentrations. Biomass concentration (reported as DW) gradually increased, and NO_3^- -N decreased proportionally throughout the batch growth experiment. The trends were hardly affected by the starting Pi concentration, even though Pi in the bulk solution was below detection by 4 h in the low-Pi experiment, but was ≥ 1 mg P/L throughout the high-Pi experiment. Thus, *Synechocystis* continued to grow well whether or not Pi was available in the bulk solution. This trend mirrors the results of Zhou et al. (2017c), showing that Pi was rapidly adsorbed to EPS, which then became a source of Pi for uptake and synthesis when bulk Pi was depleted. It also mirrors Straka and Rittmann (2017), who showed that *Synechocystis* maintained its biomass-growth rate in the absence of detectable Pi, but the biomass had progressively lower P content.

Production of SMP and EPS Figure 2 shows the concentrations of SMP, EPS, protein, and carbohydrate in SMP and EPS for both batch experiments. SMP and EPS increased in parallel to the growth of biomass (Fig. 1), but the dynamics differed, especially for SMP. The concentration of EPS was higher than SMP for the two starting Pi concentrations, but the gap narrowed with increasing incubation time, since hydrolysis of EPS is the major source of SMP (Laspidou and Rittmann 2002). Production of protein and carbohydrate mirrored the increases of SMP and EPS. The carbohydrate fraction in SMP was higher than protein, but the opposite occurred in EPS, a trend that is consistent with previous studies (Ramesh et al. 2006; Zhou et al. 2017c) that showed that carbohydrates accumulated in SMP, while protein became predominant in EPS.

Because SMP are soluble and biodegradable, they are the carbon sources and electron-donor substrates for the growth of heterotrophic bacteria (Laspidou and Rittmann 2002). Because Pi had minimal effect on the accumulation of SMP and EPS, Pi did not influence the growth of heterotrophic bacteria by altering the amount of electron-donor substrate during the batch growth of *Synechocystis*.

Production of intracellular organic matter Figure 3 shows the concentrations of total IPS and intracellular carbohydrate, protein, lipid (as FAME), chlorophyll, and carotenoid for the batch experiments. Depletion of Pi made little difference for the accumulation of total IPS or intracellular protein, carbohydrate, chlorophyll, and carotenoid. However, depletion of Pi had a strong impact on intracellular lipid, with the P-depleted culture having increasingly less intracellular lipid. Zhou et al. (2017c) proposed a set of transformation pathways for phosphorus based on a complete phosphorus mass balance during the growth of *Synechocystis*. They also found that a low starting Pi concentration led to a low organic phosphorus concentration in the extracellular and intracellular phosphorus pools of *Synechocystis*. P is an essential component of phospholipids and large amounts of organic phosphorus were

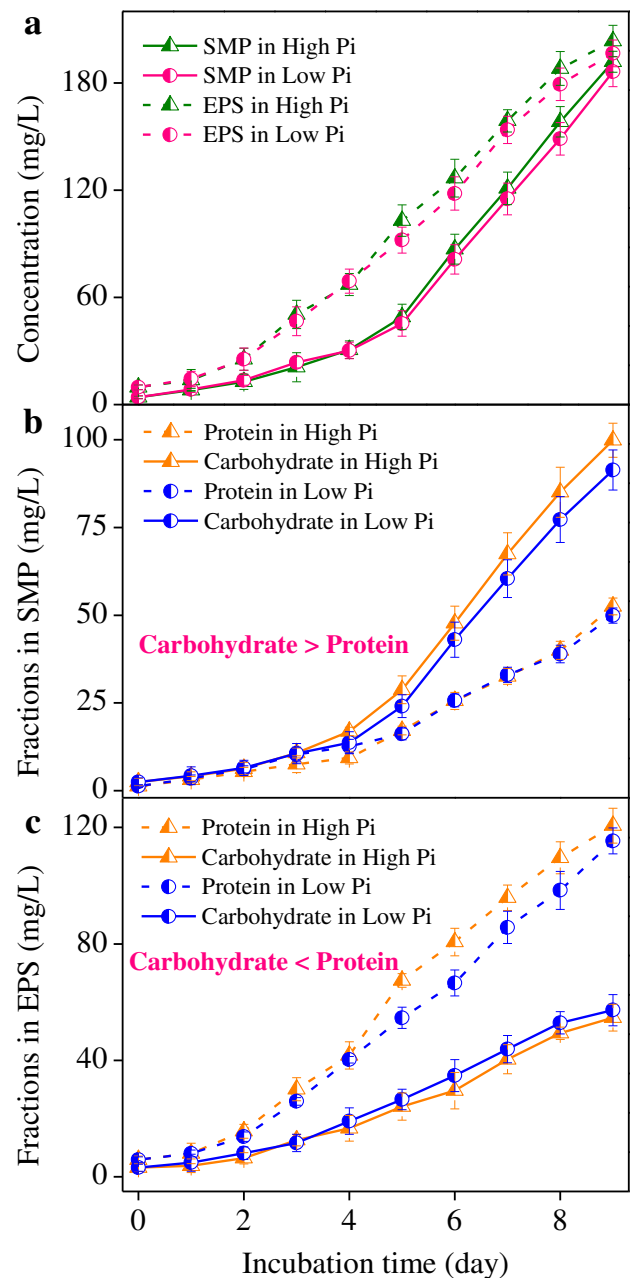


Fig. 2 Productions of soluble microbial polymers (SMPs) and extracellular polymeric substances (EPSs), along with their corresponding protein and carbohydrate contents, during batch growth of *Synechocystis* with low or high inorganic phosphate (Pi). The symbol and bars show the mean \pm SD, $n = 3$

presented as lipids in *Synechocystis* (Juneja et al. 2013); hence, a lack of available Pi led to the decrease of newly synthesized lipids.

Influences of Pi on the succession of microbial community

Figure 4 shows the unweighted PCoA for the batch experiments. One important trend is that samples from the reactor with depleted Pi clustered with low values along the PC1 axis.

Fig. 3 Effects of initial inorganic phosphate (Pi) concentration on the productions of intracellular polymeric substances (IPSS) and intracellular carbohydrate, protein, lipid, chlorophyll, and carotenoid for high- and low-Pi experiments. Symbols and bars are the \pm SD, $n = 3$; non-visible bars indicate that the SD is smaller than the size of the symbol

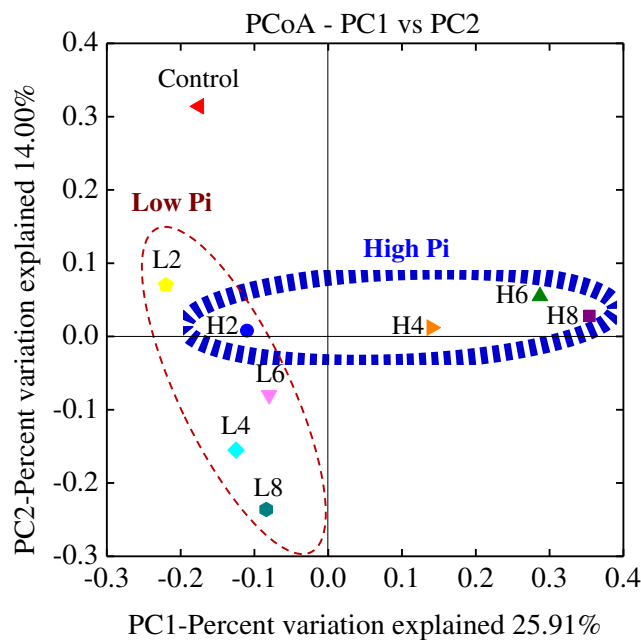
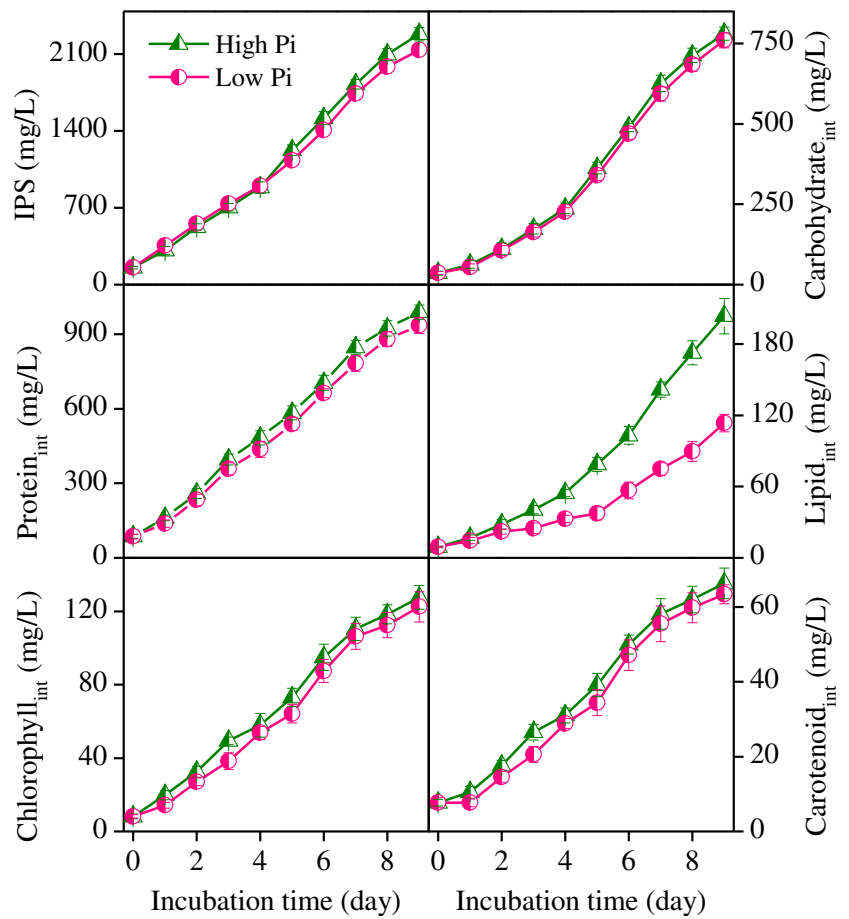


Fig. 4 PCoA, based on the unweighted UniFrac analysis, showing the evolution of microbial communities after addition of high or low initial Pi concentration. The symbols H2, H4, H6, H8, L2, L4, L6, and L8 represent the samples incubated for 2, 4, 6, and 8 days in high Pi concentration (H) and low Pi concentration (L)

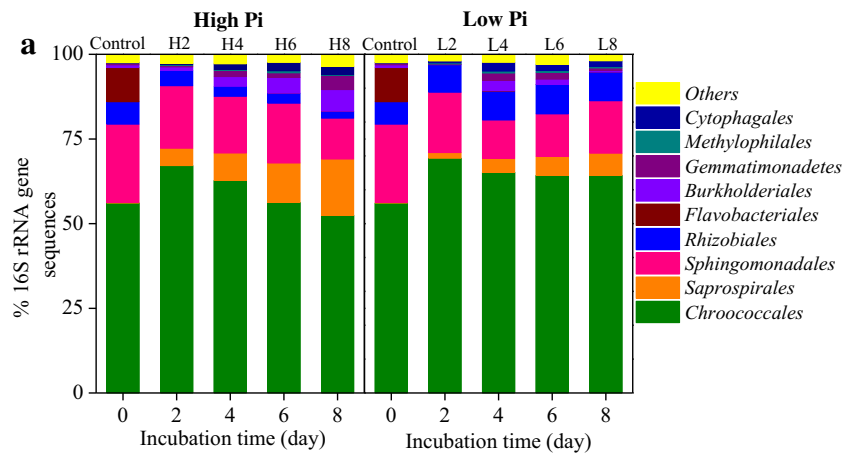
A secondary trend is that Pi depletion led to a strong time-dependent decline along the PC2 axis. In contrast, ample Pi led to a strong time-related trend along the PC1 axis.

Figure 5 further shows the microbial community structure for the batch experiments based on the unweighted UniFrac analyses at the order level. The inoculum's 16S rDNA contained 56% *Chroococcales*, belonging to Cyanobacteria and including *Synechocystis*. *Chroococcales* continued to be the largest order, it gradually increased in the initial 2 days, and low or high Pi made no difference. Important heterotrophic bacteria were *Shingobacteriales* (~23%), *Flavobacteriales* (~10%), and *Rhizobiales* (~7%).

For high Pi, *Chroococcales* gradually decreased after 2 days, while the 16S rDNA of heterotrophs gradually increased, reaching as much as 44% of the 16S rDNA after 8 days for high Pi. *Saprosirales* and *Burkholderiales* gradually increased, up to ~17% and ~6%, respectively, at the end of experiment.

For low Pi, *Chroococcales* slightly decreased after 2 days, but then remained stable after Pi was depleted. In contrast to the increase in heterotrophs for high Pi, the 16S rDNA of heterotrophs remained at about 33% for low Pi. By using fluorescence-activated cell sorting and microscopy, Zhou et al. (2018) quantified the accumulation of heterotrophic

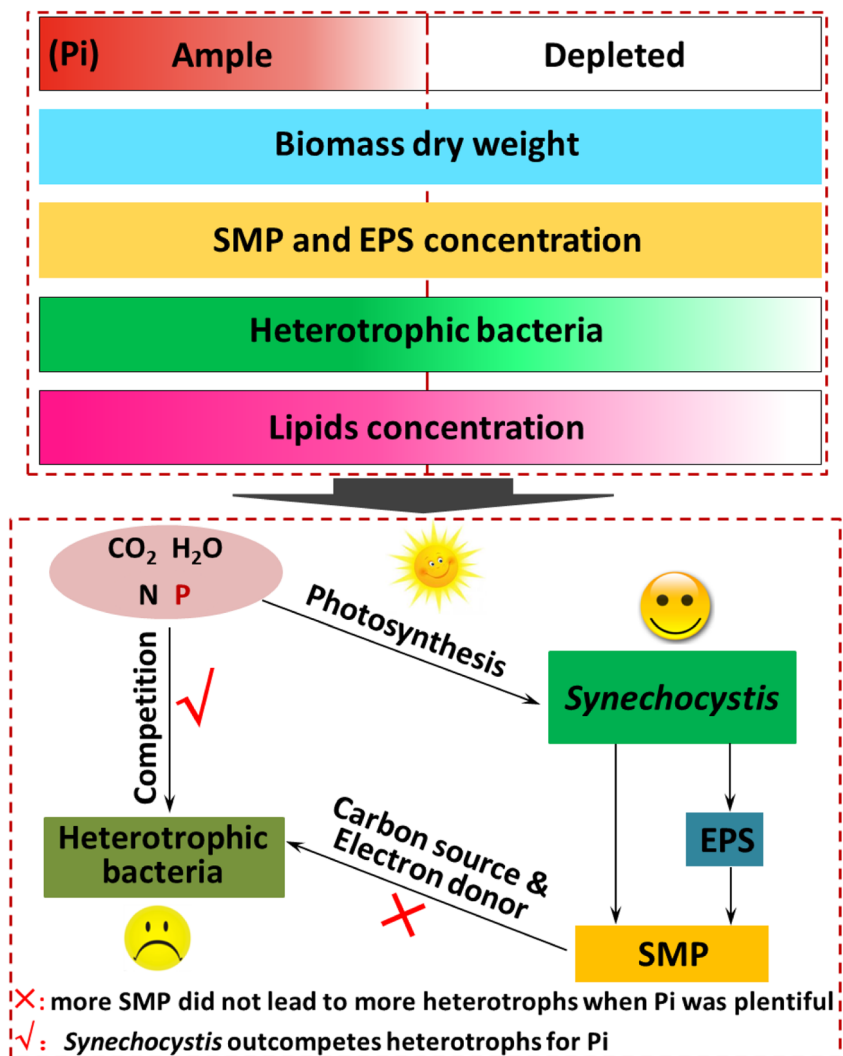
Fig. 5 Relative abundances of the 16S rDNA for bacteria at the order level based on the unweighted UniFrac analyses of the microbial community structure. The symbols of H2, H4, H6, H8, L2, L4, L6, and L8 represent the samples incubated for 2, 4, 6, and 8 days in high Pi concentration (H) and low Pi concentration (L)



bacteria during the growth of *Synechocystis*. They found that the count proportions of heterotrophic bacteria were significant (3–13%) and that depletion of Pi in the culture favored *Synechocystis* over heterotrophic bacteria. Additionally,

depletion of Pi favored *Spingobacteriales* and *Saprospirales* but disfavored *Burkholderiales*, which might be due to their different Pi affinities. Wu et al. (2013) found that *Betaproteobacteria*, containing *Burkholderiales*, played a

Fig. 6 Synthesis of mechanisms about how phosphate depletion affects lipid content and accumulation of heterotrophic bacteria during growth of *Synechocystis* sp. PCC 6803. The deeper color and white color in a bar in the top panel signify the high and low values of the parameters, respectively



key role in phosphorus removal, and Pi depletion may have led to the decrease of *Burkholderiales* for this reason. The gradual increase of SMP and EPS over time in the batch experiments favored *Sphingobacteriales* and *Saprospirales*, which are known for their wide-ranging catabolic capacities for diverse organic substrates (Whitman et al. 2016; Xia et al. 2017).

Discussion

Figure 6 synthesizes the mechanisms about how phosphate depletion affects lipid content and accumulation of heterotrophic bacteria during growth of *Synechocystis*. Pi depletion significantly affected the amount of heterotrophs and the structure of the heterotrophic community (Figs. 4 and 5). The impact on heterotrophs did not come from a change in the concentration of their organic substrate, because depletion of Pi had minimal impact on SMP and EPS accumulations (Fig. 2). Instead, the effect on heterotrophs was due to *Synechocystis* being capable of scavenging Pi at a very low concentration (Straka and Rittmann 2017). Thus, *Synechocystis* could out-compete the heterotrophs for limited Pi, even though the heterotrophs had ample electron-donor substrate in the form of SMP from *Synechocystis*. A second competitive advantage for *Synechocystis* was its ability to adapt to depleted Pi by lowering its lipid content by diverting P away from phospholipid synthesis (Juneja et al. 2013).

Based on an average *Synechocystis* cell diameter of 2 μm (Nguyen 2015), it has a biovolume of $\sim 4.2 \mu\text{m}^3$, while the typical bacteria found in the culture has a biovolume of $0.22 \mu\text{m}^3$ (Kuwae and Hosokawa 1999). Zhou et al. (2018) reported that the count proportions of heterotrophic bacteria were significant (3–13%) with the Pi concentration of 8.6 mM (same value with this study). This indicates that the cell count fraction of 3–13% for heterotrophic bacteria would represent only 0.16–0.78% of the total biomass. Thus, depleting Pi had minimal impact on the production of total biomass, which was dominated by *Synechocystis*.

The fact that Pi depletion made little difference for the production of total biomass, but lowered the relative numbers of heterotrophs, suggests that reducing the Pi concentration in the medium may be a means for minimizing the accumulation of heterotrophs and their deleterious effects in cyanobacteria culturing. However, depleting Pi also led to lower accumulation of lipids (Fig. 3), a negative consequence in some situations. Achieving the benefits of low Pi must be balanced with the loss of lipids in situations in which lipids are a primary output. For instance, it may be undesirable to have an extended period with fully depleted Pi.

By systematically investigating the effect of Pi on the growth of biomass and microbial community, we found that depleting Pi led to markedly less lipid content and

heterotrophic biomass, along with a shift in the heterotrophic community from *Burkholderiales* to *Sphingobacteriales* and *Saprospirales*. On the other hand, depleting Pi did not compromise the production of total biomass, ESP, SMP, and most types of intracellular organic polymers. The causes of the large impacts were that *Synechocystis* was much better at scavenging a very low Pi concentration and dominated the total biomass.

Acknowledgments We thank Dr. Dong Fu at the Center of Infectious Diseases and Vaccinology, Biodesign Institute at Arizona State University, for her expertise in flow cytometry for sample quantification; and Dr. Willem Vermaas and his laboratory in the School of Life Sciences at Arizona State University for providing *Synechocystis* sp. PCC6803.

Funding This work was supported by LightWorks, Arizona State University, and in part by the National Science Foundation of China (51678422, 51378368), the National Key Project of Research and Development Plan of China (No. 2017YFC0403400) and Shanghai Tongji Gao Tingyao Environmental Science and Technology Development Foundation.

Compliance with ethical standards

Conflict of interest The authors declare that they have no conflict of interest.

Ethical approval This article does not contain any studies with human participants or animals performed by any of the authors.

References

- Association APH (1998) Standard methods for the examination of water and wastewater. American Public Health Association, Washington, DC, p 1268
- Caporaso JG, Bittinger K, Bushman FD, DeSantis TZ, Andersen GL, Knight R (2009) PyNAST: a flexible tool for aligning sequences to a template alignment. *Bioinformatics* 26:266–267
- Caporaso JG, Kuczynski J, Stombaugh J, Bittinger K, Bushman FD, Costello EK, Fierer N, Pena AG, Goodrich JK, Gordon JI (2010) QIIME allows analysis of high-throughput community sequencing data. *Nat Methods* 7:335–336
- Caporaso JG, Lauber CL, Walters WA, Berg-Lyons D, Huntley J, Fierer N, Owens SM, Betley J, Fraser L, Bauer M (2012) Ultra-high-throughput microbial community analysis on the Illumina HiSeq and MiSeq platforms. *ISME J* 6:1621–1624
- Decho AW, Visscher PT, Reid RP (2005) Production and cycling of natural microbial exopolymers (EPS) within a marine stromatolite. *Palaeogeogr Palaeoclimatol* 219:71–86
- DeSantis TZ, Hugenholtz P, Keller K, Brodie EL, Larsen N, Piceno YM, Phan R, Andersen GL (2006) NAST: a multiple sequence alignment server for comparative analysis of 16S rRNA genes. *Nucleic Acids Res* 34:394–399
- Dubois M, Gilles KA, Hamilton JK, Pat R, Smith F (1956) Colorimetric method for determination of sugars and related substances. *Anal Chem* 28:350–356
- Edgar RC (2010) Search and clustering orders of magnitude faster than BLAST. *Bioinformatics* 26:2460–2461
- Frolund B, Palmgren R, Keiding K, Nielsen PH (1996) Extraction of extracellular polymers from activated sludge using a cation exchange resin. *Water Res* 30:1749–1758

- Gilbert-López B, Mendiola JA, Fontecha J, van den Broek LAM, Sijtsma L, Cifuentes A, Herrero M, Ibáñez E (2015) Downstream processing of *Isochrysis galbana*: a step towards microalgal biorefinery. *Green Chem* 17:4599–4609
- Hu Q (2004) Environmental effects on cell composition, vol 1. Blackwell Science Ltd, Oxford
- Juneja A, Ceballos R, Murthy G (2013) Effects of environmental factors and nutrient availability on the biochemical composition of algae for biofuels production: a review. *Energies* 6:4607–4638
- Kuwaie T, Hosokawa Y (1999) Determination of abundance and biovolume of bacteria in sediments by dual staining with 4', 6-diamidino-2-phenylindole and acridine orange: relationship to dispersion treatment and sediment characteristics. *Appl Environ Microbiol* 65:3407–3412
- Laspidou CS, Rittmann BE (2002) A unified theory for extracellular polymeric substances, soluble microbial products, and active and inert biomass. *Water Res* 36:2711–2720
- Nguyen BT (2015) Photoautotrophic production of biomass, laurate, and soluble organics by *Synechocystis* sp. PCC 6803. Arizona State University
- Nguyen BT, Rittmann BE (2015) Predicting dissolved inorganic carbon in photoautotrophic microalgae culture via the nitrogen source. *Environ Sci Technol* 49:9826–9831
- Nguyen BT, Rittmann BE (2016a) Effects of inorganic carbon and pH on growth kinetics of *Synechocystis* sp. PCC 6803. *Algal Res* 19:363–369
- Nguyen BT, Rittmann BE (2016b) Electron partitioning in soluble organic products by wild-type and modified *Synechocystis* sp. PCC 6803. *Biomass Bioenergy* 90:237–242
- Ramesh A, Lee DJ, Hong SG (2006) Soluble microbial products (SMP) and soluble extracellular polymeric substances (EPS) from wastewater sludge. *Appl Microbiol Biotechnol* 73:219–225
- Rashidan KK, Bird DF (2001) Role of predatory bacteria in the termination of a cyanobacterial bloom. *Microb Ecol* 41:97–105
- Rippka R, Deruelles J, Waterbury JB, Herdman M, Stanier RY (1979) Generic assignments, strain histories and properties of pure cultures of cyanobacteria. *Microbiology* 111:1–61
- Ruiz V, Ilhan ZE, Kang DW, Krajmalnik-Brown R, Buitrón G (2014) The source of inoculum plays a defining role in the development of MEC microbial consortia fed with acetic and propionic acid mixtures. *J Biotechnol* 182:11–18
- Sheng J, Vannela R, Rittmann BE (2011) Evaluation of cell-disruption effects of pulsed-electric-field treatment of *Synechocystis* PCC 6803. *Environ Sci Technol* 45:3795–3802
- Straka L, Rittmann BE (2017) The role of heterotrophic bacteria in assessing phosphorus stress to *Synechocystis* sp. PCC6803. *J Appl Phycol* 29:1877–1882
- Wang Q, Garrity GM, Tiedje JM, Cole JR (2007) Naive Bayesian classifier for rapid assignment of rRNA sequences into the new bacterial taxonomy. *Appl Environ Microbiol* 73:5261–5267
- Wang Y, Gan N, Zhou Y, Li TH, Cao YT, Chen YJ (2017) Novel single-stranded DNA binding protein-assisted fluorescence aptamer switch based on FRET for homogeneous detection of antibiotics. *Biosens Bioelectron* 87:508–513
- Whitman T, Pepe-Ranney C, Enders A, Koechli C, Campbell A, Buckley DH, Lehmann J (2016) Dynamics of microbial community composition and soil organic carbon mineralization in soil following addition of pyrogenic and fresh organic matter. *ISME J* 10:2918–2930
- Wu DL, Shen YH, Ding AQ, Mahmood Q, Liu S, Tu QP (2013) Effects of nanoscale zero-valent iron particles on biological nitrogen and phosphorus removal and microorganisms in activated sludge. *J Hazard Mater* 262:649–655
- Xia SQ, Zhou Y, Eustance E, Zhang ZQ (2017) Enhancement mechanisms of short-time aerobic digestion for waste activated sludge in the presence of cocoamidopropyl betaine. *Sci Rep-UK* 7:13491
- Xin L, Hu HY, Gan K, Sun YX (2010) Effects of different nitrogen and phosphorus concentrations on the growth, nutrient uptake, and lipid accumulation of a freshwater microalga *Scenedesmus* sp. *Bioresour Technol* 101:5494–5500
- Zevin AS, Nam T, Rittmann B, Krajmalnik-Brown R (2015) Effects of phosphate limitation on soluble microbial products and microbial community structure in semi-continuous *Synechocystis*-based photobioreactors. *Biotechnol Bioeng* 112:1761–1769
- Zhang CF, Li QC, Fu L, Zhou DD, Crittenden JC (2018) Quorum sensing molecules in activated sludge could trigger microalgae lipid synthesis. *Bioresour Technol* 263:576–582
- Zhou Y, Nguyen BT, Lai YS, Zhou C, Xia SQ, Rittmann BE (2016) Using flow cytometry to evaluate thermal extraction of EPS from *Synechocystis* sp. PCC 6803. *Algal Res* 20:276–281
- Zhou Y, Lai YS, Eustance E, Straka L, Zhou C, Xia SQ, Rittmann BE (2017a) How myristyltrimethylammonium bromide enhances biomass harvesting and pigments extraction from *Synechocystis* sp. PCC 6803. *Water Res* 126:189–196
- Zhou DD, Zhang CF, Fu L, Xu L, Cui XC, Li QC, Crittenden JC (2017b) Responses of the microalga *Chlorophyta* sp. to bacterial quorum sensing molecules (N-acylhomoserine lactones): aromatic protein-induced self-aggregation. *Environ Sci Technol* 51(6):3490–3498
- Zhou Y, Nguyen BT, Zhou C, Straka L, Lai YS, Xia SQ, Rittmann BE (2017c) The distribution of phosphorus and its transformations during batch growth of *Synechocystis*. *Water Res* 122:355–362
- Zhou Y, Eustance E, Straka L, Lai YS, Xia SQ, Rittmann BE (2018) Quantification of heterotrophic bacteria during the growth of *Synechocystis* sp. PCC 6803 using fluorescence activated cell sorting and microscopy. *Algal Res* 30:94–100

Publisher's note Springer Nature remains neutral with regard to jurisdictional claims in published maps and institutional affiliations.